Atmos. Chem. Phys. Discuss., doi:10.5194/acp-2016-443, 2016
Manuscript under review for journal Atmos. Chem. Phys.
Published: 10 June 2016

Atmospheric Chemistry and Physics Discussions

Global and regional radiative forcing from 20% reductions in BC, OC and SO4 - an HTAP2 multi-model study

Camilla Weum Stjern[1], Bjørn Hallvard Samset[1], Gunnar Myhre[1], Huisheng Bian[2], Mian Chin[3], Yanko Davila[4], Frank Dentener[5], Louisa Emmons[6], Johannes Flemming[8], Amund Søvde Haslerud[1], Daven Henze[4], Jan Eiof Jonson[7], Tom Kucsera[9], Marianne Tronstad Lund[1], Michael Schulz[7], Kengo Sudo[10], Toshihiko Takemura[11], Simone Tilmes[6]

[1] CICERO Center for International Climate and Environmental Research, Oslo, Norway
[2] Goddard Earth Sciences and Technology Center, University of Maryland, Baltimore, Maryland, USA
[3] Earth Sciences Division, NASA Goddard Space Flight Center, Greenbelt, MD, USA
[4] Department of Mechanical Engineering, University of Colorado, Boulder, CO, USA
[5] European Commission, Joint Research Centre, Institute for Environment and Sustainability, Ispra (VA), Italy
[6] Atmospheric Chemistry Division, National Center for Atmospheric Research (NCAR), CO, USA
[7] Norwegian Meteorological Institute, Oslo, Norway
[8] European Centre for Medium Range Weather Forecast (ECMWF), Reading, UK
[9] Universities Space Research Association, Greenbelt, MD, USA
[10] Nagoya University, Furocho, Chigusa-ku, Nagoya, Japan
[11] Research Institute for Applied Mechanics, Kyushu University, Fukuoka, Japan

Correspondence to: Camilla W. Stjern (camilla.stjern@cicero.oslo.no)

Abstract

In the Hemispheric Transport of Air Pollution Phase 2 (HTAP) exercise, a range of global atmospheric general circulation and chemical transport models performed coordinated perturbation experiments with 20 % reductions in emissions of anthropogenic aerosols, or aerosol precursors, in a number of source regions. Here, we compare the resulting changes in the atmospheric load and vertically resolved profiles of black carbon (BC), organic aerosols (OA) and sulfate (SO_4) from 10 models that include treatment of aerosols. We use a set of temporally, horizontally and vertically resolved profiles of aerosol forcing efficiency (AFE) to estimate the impact of emission changes in six major source regions on global radiative forcing (RF) pertaining to the direct aerosol effect. Results show that mitigations in South and East Asia have substantial impacts on the radiative budget in all investigated receptor regions, especially for BC. In Russia and the Middle East, more than 80 % of the forcing for BC and OA is due to extra-regional emission reductions. Similarly, for North America, BC emissions control in East Asia is found to be more important than domestic mitigations, which is consistent with previous findings. Comparing fully resolved RF calculations to RF estimates based on vertically averaged AFE profiles allows us to quantify the importance of vertical resolution to RF estimates. We find that locally in the source regions, a 20 % emission reduction strengthens the radiative forcing associated with SO_4 by 25 % when including the vertical dimension, as the AFE for SO_4 is strongest near the surface. Conversely, the local RF from BC weakens by 37 % since BC AFE is low close to the ground. The influence of inter-continental transport on BC forcing, however, is enhanced by one

Atmos. Chem. Phys. Discuss., doi:10.5194/acp-2016-443, 2016
Manuscript under review for journal Atmos. Chem. Phys.
Published: 10 June 2016

Atmospheric Chemistry and Physics Discussions

third when accounting for the vertical aspect, because long-range transport leads primarily to aerosol changes at high altitudes, where the BC AFE is strong.

1. Introduction

Atmospheric aerosols have a range of effects on the atmosphere, biosphere and on human beings. They significantly alter the global radiative balance, through processes spanning from direct interaction with sunlight (Myhre et al., 2013; Yu et al., 2006) to modification of cloud properties (Lohmann and Feichter, 2005; Stevens and Feingold, 2009) and influences on thermal stability (Koch and Del Genio, 2010). Aerosols have also been shown to affect regional precipitation (Liu et al., 2011; Khain, 2009) and atmospheric circulation patterns (Bollasina et al., 2011). In addition to climatic impacts come the adverse effects that aerosol pollution has on human health (Janssen, 2012; Geng et al., 2013). Changes in aerosol emissions are therefore of interest both for climate and public health policies (Shindell et al., 2012), which makes it imperative to provide precise estimates of aerosol effects on these outcomes. However, present day emissions have high spatial and temporal variability, and acquiring accurate measurements is a challenge. Similarly, aerosol atmospheric lifetimes and processes leading to long-range transport are insufficiently quantified. The total anthropogenic aerosol radiative forcing (RF) since the onset of the industrial period counters large parts of the positive RF from CO_2 and other greenhouse gases, and was recently evaluated to be –0.9 W m^{-2} with a 95 % uncertainty interval from –1.9 to –0.1 W m^{-2} (Boucher et al., 2013). Of the total aerosol RF, the direct short-wave aerosol radiative interaction contributed with –0.35 W m^{-2}, with an uncertainty interval of –0.85 to +0.15 W m^{-2}. These large uncertainty intervals imply that the RF from aerosols is poorly constrained. Likewise, there is still a large divergence between model- and satellite-derived surface particulate matter and observed concentrations (Brauer et al., 2016).

One specific uncertainty in calculating aerosol RF is connected to the vertical distribution of aerosols. The radiative impact of an aerosol depends on its absorbing and reflecting properties, but these properties, as well as their radiative impact, are subject to modifications by variable atmospheric conditions. For instance, relative humidity has a large impact on the scattering properties of light reflecting aerosols (Fierz-Schmidhauser et al., 2010; Haywood and Shine, 1997). Also, the efficiency of absorbing aerosols is augmented with increasing quantities of underlying clouds and gases that reflect solar radiation back onto the aerosols, thereby enhancing their absorption (Zarzycki and Bond, 2010). Meanwhile, competition with other processes such as Rayleigh scattering and radiative interactions of other aerosol species (Samset and Myhre, 2011) may dampen the radiative impact of an aerosol. As these factors typically vary with altitude, so will the aerosols' forcing efficiency. Accurate knowledge on the vertical distribution of aerosol load is therefore important (Ban-Weiss et al., 2011; Samset and Myhre, 2015; Vuolo et al., 2014; Zarzycki and Bond, 2010). Presently, the atmospheric models that simulate the climate impact of aerosols have substantial variations in their vertical distribution of aerosols. In fact, results from the recent AeroCom Phase II multimodel exercise (Samset et al., 2014; Samset et al., 2013) show that differences in vertical profiles gave rise to between 20 % and 50 % of the intermodel differences in direct RF estimated from common BC emissions from fossil fuel and biofuels (FF+BF).

Due to long-range atmospheric transport, emissions in major source regions may have widespread health and climate impacts that go far beyond the domestic domain. Studies of long-range transport of aerosols have found that the vertical distribution of aerosols in the source region has important implications to the magnitude and spatial extent of their climate impact – not only because of the variation of forcing efficiency with height, but because the strong large-scale winds in the upper

Atmos. Chem. Phys. Discuss., doi:10.5194/acp-2016-443, 2016
Manuscript under review for journal Atmos. Chem. Phys.
Published: 10 June 2016

troposphere can transport aerosols for particularly long distances if they reach these levels. For instance, Liu et al. (2008) found in a study of Cloud-Aerosol Lidar and Infrared Pathfinder Satellite Observations (CALIPSO) measurements that the higher Saharan dust aerosols were lifted up in the source region, the further they were carried across the Atlantic Ocean. Similarly, Huang et al. (2008) studied long-range transport from Asia during the Pacific Dust Experiment (PACDEX) and found indications of aerosol transport via upper tropospheric westerly jets – the efficiency of which was influenced by the vertical distribution of Asian dust in the free troposphere of the source region.

These studies underline the need for a better understanding of how variations between atmospheric models contribute to the uncertainties in radiative forcing estimates, and specifically the role of different vertical distribution of aerosols to these uncertainties. In 2005, the Task Force on Hemispheric Transport of Air Pollution (TF HTAP) was established under the United Nations Economic Commission for Europe (UNECE) Convention on Long- Range Transboundary Air Pollution (LRTAP Convention). One of its goals is to further our understanding of aerosol intercontinental transport, and assess impacts of emission changes on air quality, climate, and ecosystems (http://www.htap.org/). The climate impact of aerosol emission reductions in four large source regions was investigated for a series of model simulations from the first phase of the HTAP Task Force (HTAP1) by Yu et al. (2013), who calculated radiative forcing as a product of aerosol optical depth and an aerosol forcing efficiency (AFE) estimated using the Goddard Chemistry Aerosol Radiation and Transport (GOCART) model. They found that, on average, the global direct radiative forcing of SO_4, particulate organic matter and black carbon was lowered about 9 %, 3 % and 10 %, respectively, when all anthropogenic emissions where reduced by 20 % in North America, Europe, South Asia or East Asia. Together, the four-region total emissions accounted for 72 %, 21 % and 46 % of global emissions for SO_4, particulate organic matter and black carbon, respectively. Inter-model differences were found to be substantial, in part because the models were using different emission inventories in their simulations.

The present study utilizes model experiments organized by the second phase of the TF HTAP (HTAP2). We focus on the six priority source regions (Fig. 1) selected by the TF HTAP for HTAP2: North America (NAM), Europe (EUR), South Asia (SAS), East Asia (EAS), Russia/Belarussia/Ukraine (RUS) and the Middle East (MDE). Note that while the first four regions are similar to those investigated by Yu et al. (2013), the HTAP2 regions are defined by geopolitical boundaries while the HTAP1 regions were larger and included more ocean areas. We aim to explain how much a 20 % emission reduction in these source regions would impact other regions in terms of aerosol burden and radiative forcing changes. To estimate the climate impacts of the mitigations we calculate radiative forcing based on column averaged aerosol fields and AFE estimates in a method equivalent to Yu et al. (2013) (here, using the OsloCTM2 model), but extend the analyses to also involve 4D AFE and aerosol burden profiles. This allows us to quantify how the vertical distribution of aerosols influences the potential impact of regional emission mitigation strategies.

In the next section, we will go through our methods. Section 3 presents the results, starting with changes in aerosol concentrations for the different experiments, and moving on to resulting changes in radiative forcing as well as the influence of inter-continental transport. The results are summarized in Sect. 4.

Atmos. Chem. Phys. Discuss., doi:10.5194/acp-2016-443, 2016
Manuscript under review for journal Atmos. Chem. Phys.
Published: 10 June 2016

2. Methods

2.1 The HTAP2 experiments and models

As part of the HTAP2 exercise, global aerosol-climate CTMs and GCMs performed a baseline (*BASE*) simulation with climate and aerosol emissions corresponding to present day (year 2010) conditions (Koffi, 2016). Anthropogenic emissions followed Janssens-Maenhout et al. (2015). Each model also ran simulations with all anthropogenic emissions reduced by 20 % in a selection of source regions. We have chosen to focus on the six priority source regions pointed out by the TF HTAP and shown in Fig. 1 (a). The experiments where all anthropogenic emissions are reduced by 20 % in the NAM, EUR, SAS, EAS, RBU and MDE regions are referred to correspondingly as *NAMreduced*, *EURreduced*, *SASreduced*, *EASreduced*, *RBUreduced* and *MDEreduced*. We will additionally analyze emission reduction influences on the Arctic receptor region, also marked in Fig. 1 (a).

The present study takes input from ten global aerosol models, listed in Table 1 along with core parameters and references. Horizontal and vertical resolutions of the models are also indicated in Table 1. The time resolution of output used in this study is monthly for all models, although models were run at finer resolution. To be included here, we required that the models had provided 3D, temporally resolved mass mixing ratios of atmospheric aerosols for both the baseline and at least four of the reduced emission scenarios.

The analyzed aerosol species include sulfate (SO_4), organic aerosols (OA) and black carbon (BC). A limitation of the current analyses of OA is that while some models reported OA directly, others gave emissions and concentrations of OC instead (see Table S-1). OC can be converted to OA through multiplication by an OC-to-OA conversion factor, which varies with source, aerosol age and the presence of other chemical species (see e.g. Tsigaridis et al. (2014) and references therein). However, due to limited level of detail in the available model data, as well as due to consistency to the method used in Chin et al. (manuscript in preparation), we multiplied all OC values by a factor 1.8 to obtain OA. As some of the models have included secondary organic aerosols (SOA) in their OA values while other have not, this approximation likely leads to additional inter-model variability.

Model output was provided as mass mixing ratio (MMR, unit of µg/kg), but we have also analyzed the data in terms of column integrated aerosol abundance. The conversion from MMR to abundance was done by interpolating the MMR fields from each model to the resolution of one host model (OsloCTM2) with a vertical resolution of 60 layers, using pressure and mass of air distributions from that model and summing over all layers. See e.g. Samset et al. (2013) for a detailed description of this method.

2.2 Estimating radiative forcing

In order to estimate the radiative forcing resulting from the emission reductions simulated by the HTAP2 experiments, we utilize precalculated 4D distributions of aerosol forcing efficiency (AFE), which is defined as the RF per gram of a given aerosol species. For the three aerosol species, AFE was calculated for each grid cell and month through a series of simulations inserting a known amount of aerosol within a known background of aerosols and clouds, and calculating its radiative effect using an 8-stream radiative transfer model (Stamnes et al., 1988). Aerosol optical properties were derived from Mie theory. The absorption of aged BC was enhanced by 50% to take into account external mixing. Hygroscopic growth of SO_4 was included, scaling with relative humidity. For OA, purely scattering aerosols are assumed. Background aerosols were taken from simulations using OsloCTM2. See

Atmos. Chem. Phys. Discuss., doi:10.5194/acp-2016-443, 2016
Manuscript under review for journal Atmos. Chem. Phys.
Published: 10 June 2016

Samset and Myhre (2011) for details, but note that all numbers have been updated since that work, taking into account recent model improvements (Samset and Myhre, 2015). The resulting AFE profiles, averaged over the individual regions from Fig. 1 (a), is presented in Sect. 3.3. This method is equivalent to what is sometimes termed a radiative kernel calculation. For a discussion on the impact on radiative forcing from using a single model kernel, see Samset et al. (2013).

The direct RF from a given aerosol species due to a 20 % emission reduction was then estimated by multiplying the resulting aerosol burden change profile ΔBD with the AFE distribution for that species and point in space and time:

$$RF(lon, lat, lev, time) = \Delta BD(lon, lat, lev, time) \times AFE(lon, lat, lev, time) \quad (1)$$

The RF calculated at each model level using this method should be interpreted as the radiative forcing exerted at top of the atmosphere (TOA), due to the aerosol abundance within that layer.

In this procedure, cloud fields, surface albedo and background aerosols, all of which may influence global and annual mean RF, are prescribed to the AFE distribution. Hence, intermodel variability will likely be lower using this method than if the models had provided their own estimates of RF. Further, the absolute RF will be influenced by the mean efficiency of the host model (OsloCTM2). As recently shown in the AeroCom Phase II model intercomparison (Myhre et al., 2013), OsloCTM2 is among the models with strongest global, annual mean AFE values for BC and OA, in part due to the heightened complexity of the radiation scheme used (Myhre and Samset, 2015). For SO_4, the AFE of OsloCTM2 is close to the AeroCom median.

As will be shown below, there are significant differences between the vertical profiles of aerosol abundance predicted by the participating models. To estimate the effect of these differences on global, annual mean RF, we also compute the radiative forcing in a way that does not account for the vertical aerosol distributions: we average out the vertical dimension by calculating column aerosol burdens and multiply by corresponding vertically averaged AFE distributions from OsloCTM2, which utilized the specific vertical aerosol distribution of that model.

$$RF_{3D}(lon, lat, time) = \Delta BD(lon, lat, time) \times AFE(lon, lat, time) \quad (2)$$

Here, RF_{3D} indicates a radiative forcing estimate where the two horizontal dimensions, as well as time, is included, but where the vertical dimension is averaged out. For further details on the above method, see Samset et al. (2013).

2.3 Response to extra-regional emission reductions

The impact of intercontinental transport between regions is investigated through calculating the Response to Extra-Regional Emission Reductions (RERER). While this metric is originally defined in HTAP (2010) to study the influence of inter-continental transport on region average burden change or surface concentrations, we utilize a version of the RERER defined in HTAP (2010) studying instead the influence on forcing:

$$RERER_{sr} = \frac{\Delta RF_{base,global} - \Delta RF_{base,sr}}{\Delta RF_{base,global}} = \frac{(RF_{base} - RF_{global}) - (RF_{base} - RF_{sr})}{RF_{base} - RF_{global}} \quad (3)$$

Here, *base* refers to the base simulation with no emission reductions, *global* refers to an experiment where anthropogenic emissions all over the globe are reduced by 20 %, and *sr* refers to the experiment

Atmos. Chem. Phys. Discuss., doi:10.5194/acp-2016-443, 2016
Manuscript under review for journal Atmos. Chem. Phys.
Published: 10 June 2016

where emissions in source region *sr* are reduced by 20 %. RERER is then calculated for all source regions and species. A low RERER value means that the forcing within a region is not very sensitive to extra-regional emission reductions.

In addition to the above calculation of RERER for RF, we also calculate RERER for changes in total column aerosol burden, which gives an estimate of inter-continental transport when disregarding the vertical dimension.

3. Results and discussion

In the following sections, we first present the global and regional aerosol burdens simulated by the participating models in response to the baseline emissions, before moving on to showing the local and remote burden changes due to 20 % reduction in regional emissions. Then, we show the calculated radiative forcing from these burden changes, and discuss how regional aerosol mitigation efforts may impact local and remote regions.

3.1 Baseline aerosol burdens and emissions

Figures 1 (b) – (d) show the multi-model median column integrated burden fields for BC, OA and SO_4, respectively, for the unperturbed *BASE* simulation. The source regions of focus in this study are mostly recognized as regions of high aerosol burden in the maps, as are other regions such as Central Africa and South America (high BC and OA from open biomass burning). Areas with significant loads can also be seen over global oceans, far from the main emission regions, showing the importance of long-range aerosol transport for both the global and regional climate impact of aerosols.

In Table 2, the regional averages of aerosol burdens for the four source regions reveal some differences between the regions. Particularly, for BC and OA, East and South Asia have significantly higher burdens than North America, Europe, Russia/Belarussia/Ukraine (henceforth referred to as Russia, for simplicity) and the Middle East. For SO_4, the Middle East ranks among the high-emission source regions. The source regions are also different in terms of meteorology (see Table 2) and surface albedo (not shown), which will influence the local as well as remote effects of emission reductions. For instance, the amount, timing and intensity of precipitation events largely controls the rate of wet removal of fresh aerosols. For year 2010 the average daily precipitation in the Middle East was 0.4 mm/day, while in South Asia it was 3.3 mm/day (Table 2). Meanwhile, the South Asian region is also marked by a significantly higher convective mass flux than the other regions, which likely enhances long range transport due to convective lifting of insoluble aerosols to high altitudes. The fractions of BC, OA and SO_4 to the total BC+OA+SO_4 sum are on the other hand quite similar between the regions, with BC contributing 4-8 % of the total, OA contributing 25-45 % of the total, and SO_4 contributing 51-70 % of the total (not shown). Europe has a lower fraction of OA and a higher share of SO_4 than the other regions, while the Middle East has a lower BC fraction and higher SO_4 fraction.

Regionally and annually averaged emissions (top row of Fig. 2) for all three aerosol species are highest in East Asia. The error bars indicate the full range of model results. For BC and SO_4 there is a very limited spread between the models, as all HTAP2 model groups used emission data from the Emissions Database for Global Atmospheric Research (EDGAR) HTAP_v2 emission inventory (Janssens-Maenhout et al., 2015). However, there is a large spread in OA emissions between the models, primarily due to high OA emissions from GEOS5, GEOSCHEMADJOINT and GOCART, but perhaps also linked to the above mentioned conversion from OC to OA for some of the models.

Atmos. Chem. Phys. Discuss., doi:10.5194/acp-2016-443, 2016
Manuscript under review for journal Atmos. Chem. Phys.
Published: 10 June 2016

In spite of the unified emissions, total aerosol burdens (not shown) vary substantially between the models. This is expected, as there is a broad range of model processes that connect emissions to global aerosol burden, and different models treat these processes differently. For example, the convection schemes used by the different models listed in Table 1 differ markedly. Parametrizations of processes such as wet removal and oxidation will also be sources of inter-model difference, as will their horizontal and vertical resolution. For instance, Molod et al. (2015) performed model simulations of different horizontal resolution with the GEOS5 model, which parameterizes convection using the relaxed Arakawa-Schubert algorithm (RAS). They found that the mass flux decreases with increasing resolution, resulting in reduced low-level drying, which again might increase wet removal and lower the aerosol burden. Kipling et al. (2015) investigated processes important for the shape of vertical aerosol profiles by performing a number of sensitivity tests using the HadGEM3-UKCA model, and comparing the variation in results to the inter-model variation from the AeroCom Phase II control experiment. They found that the vertical profile was controlled mainly by convective transport, in-cloud scavenging and droplet growth by condensation – processes that have widely different parametrizations between models.

An HTAP2 model-observation comparison study by Chin et al. (manuscript in preparation) finds that in general, compared to measurements, the two CHASER models typically report too high surface concentrations of SO_4, OA and BC, while OsloCTM3 generally have low values. Figure 3 shows vertically resolved plots of globally averaged mass mixing rations (MMR) for the three aerosol species, and illustrates that the high values for CHASERT42 and CHASERT106 extend through all vertical layers. It is interesting to note that the CHASER models use a version of the Arakawa-Schubert parametrization of convection, and that the highest-resolution version (T106) has the lowest aerosol burden among the two, which could be related to the findings of Molod et al. (2015) noted above. Note that for SO_4, GOCART and GEOS5 have particularly high MMR aloft, see Fig. 3 (c).

3.2 Aerosol changes

The middle row of Fig. 2 shows the change in global, annual mean aerosol burden following a 20 % emission reduction in the region noted on the x axis. The burden change is clearly highest for the regions with the highest baseline emissions (top row of Fig. 2). The ranges are wider, particularly in the tropical regions, since, as commented above, the processes connecting emissions to burdens vary greatly between the models. The inter-model spread becomes even clearer when expanding the vertical dimension. This is illustrated by Fig. 4, which shows globally averaged vertical profiles of aerosol MMR change per vertical layer for all species, experiments and models. Differences in the vertical profiles, reflecting differences in vertical transport, between the models can be seen. SPRINTARS and the two CHASER models report among the highest MMR changes. For BC, SPRINTARS have particularly large MMR changes for the *RBUreduced* and *MDEreduced* experiments.

The *SASreduced* experiment (third row, Fig. 4) is associated with the most pronounced upper-level MMR changes, conceivably because this is the region associated with highest convective activity. Indeed, the average upward moist convective mass flux in the SAS region is more than double what it is in for instance the North American region (Table 2). Possibly linked to the treatment of convection in the models, we find that GOCART, GEOSCHEMADJOINT and GEOS5 show particularly high upper-level BC changes from emission perturbations in the SAS region. One common denominator for these two models is the use of the above mentioned RAS algorithm, which in a study based on an earlier version of the GEOS model was found to overestimate convective mass transport (Allen et al.,

Atmos. Chem. Phys. Discuss., doi:10.5194/acp-2016-443, 2016
Manuscript under review for journal Atmos. Chem. Phys.
Published: 10 June 2016

1997). However, while GEOS5 also has large high-altitude burden changes for both OA and SO_4 for the *SASreduced* experiment, GOCART and GEOSCHEMADJOINT show very weak high-altitude changes compared to the other models in the SO_4 case. Conceivably, wet scavenging, to which SO_4 is more subject than BC, is stronger in GOCART than in other models over this region.

Regional increases in aerosol concentrations imposed by emission reductions can be observed for SPRINTARS and CAMchem, and to a smaller extent also for the CHASER models, GEOS5 and C-IFS (not shown, but visible in the globally averaged *RBUreduced* and *MDEreduced* plots for OA in Fig. 4). This may at least partly be linked to nudging, which is a simple form of data assimilation that adjusts certain variables of free running climate models to meteorological re-analysis data – in this case, to constrain the climate to year 2010 meteorology. The nudging is done differently by the individual model groups. For instance, in SPRINTARS there is no nudging below altitudes of approximately 300 m, which means that the meteorological field will be slightly different due to perturbed aerosol effects between the two experiments. Nudging has been shown to have the potential to induce forcings that could change the base characteristics of a model; Zhang et al. (2014) demonstrated using the CAM5 model that nudging towards reanalysis data resulted in a substantial reduction in cold clouds.

We have also calculated regional averages of the MMR change profiles for the regions in Fig. 1 (a), see Fig. 5. The figure shows the rate of MMR change in a receptor region (colored lines) caused by emission reductions in a source region (rows), for the three aerosol species (columns). These figures clearly show the effect of long-range aerosol transport on vertical aerosol profiles: notice for instance the SO_4 burden change profile (rightmost column) for the Arctic (light grey), which reaches a maximum at relatively low altitudes for North American emission changes (first row), but high up for South Asian emission changes (third row).

3.2.1 Aerosol lifetime

Referring to Fig. 2, we have in the bottom row estimated the regional, annually averaged atmospheric lifetime of the different aerosol species emitted from the six regions, through the relation

$$\tau = \Delta BD(Tg)/\Delta Em(Tg\ day^{-1}) \quad (4)$$

where ΔEm is the change in emissions on daily timescale within the region (and hence also the global change), and ΔBD is the resulting change in global aerosol burden. SO_4 has an estimated lifetime of 4-6 days, except for emissions in the MDE region where the model mean lifetime is 10 days, with an inter-model spread from 8 (GOCART) to 17 (CHASERre1) days, corresponding to the models with the lowest and highest SO_4 MMR changes, respectively. OA has slightly higher lifetimes around 8 days, except for the MDE regions where the lifetime is above 20 days. This is high compared to the AeroCom model comparison of Tsigaridis et al. (2014), which found a median global OA lifetime of 5.4 days (range 3.8–9.6 days). Note that fewer models performed the *MDEreduced* and *RBUreduced* experiments (see Table S-5) and so the estimates for these regions are much more uncertain. BC lifetimes are typically around 12 days for emissions in the MDE and SAS regions and 7 days in the other regions, which is also slightly higher than the 5 days shown by Samset et al. (2014) to be an upper limit for reproducing remote ocean BC observations. The extended lifetime for aerosols emitted within the SAS region is likely due to more efficient vertical mixing (see Table 2) and low precipitation except during the monsoon season. This finding is consistent with previous studies and the longer lifetime is seen particularly during Northern hemisphere winter (Berntsen et al., 2006).

Atmos. Chem. Phys. Discuss., doi:10.5194/acp-2016-443, 2016
Manuscript under review for journal Atmos. Chem. Phys.
Published: 10 June 2016

High lifetimes in the MDE region, particularly for OA and SO_4 which are more subject to wet removal, are probably linked to dry atmospheric conditions (see Table 2).

3.3 Radiative forcing changes

In Fig. 6 we show annual and regional averages of the AFE profiles used as input to the RF calculations (Samset and Myhre, 2011), for the regions in Fig. 1 (a). Underlying calculations were performed on grid-level using separate profiles for each aerosol species. In panel (a), the global, annual mean BC AFE increases strongly with altitude for all regions, rising from about 400 Wg^{-1} close to the surface to about 3700 Wg^{-1} at top-of-atmosphere (TOA). The reason for this increase is mainly scattering and reflection from underlying clouds, gases and aerosols, the cumulative amount of which increases with altitude. This enhances the amount of short wave radiation that the BC aerosol may absorb, and therefore its radiative impact increases with height. Hence, a given change in BC concentration will have a larger influence on the total TOA forcing if it occurs at high altitudes than if it occurs at lower altitudes. Note that the magnitude as well as the exact shape of the profile varies between the regions, depending on geographic location, climatic factors and surface albedo. For instance, the high surface albedo of the Arctic or the Middle East renders the radiative impact of the dark BC aerosols, and therefore the AFE magnitude, particularly high.

Panels (b) and (c) show similar curves for OA and SO_4 respectively, with a weaker dependency on altitude compared to BC. For SO_4, a strong maximum close to 900hPa can be seen, mainly related to humidity and hygroscopic growth (Samset and Myhre, 2011) which significantly enhances the scattering properties of SO_4 aerosols (Haywood et al., 1997; Myhre et al., 2004; Bian et al., 2009), but which is less relevant for OA. This is well illustrated by looking at the regionally averaged relative humidity from MERRA data in Fig. 7, which shows that the Middle East, which has a weak relative humidity (RH) profile (as well as low average cloud cover; Table 2), is the region with the weakest SO_4 AFE profile. Meanwhile, remote ocean regions typically associated with persistent low-level clouds (e.g. the South Atlantic or the North/South Pacific) are the areas with the most pronounced SO_4 AFE profiles (not shown).

Combining these AFE profiles with aerosol burden changes for each grid cell, month and vertical level (see Eq. (1)), we obtain direct radiative forcing. Table 3 shows the global mean direct RF, per Tg emission change, for the three species and six experiments. The forcing ranges between 51.9 and 210.8 mWm^{-2} Tg^{-1} for BC, between -2.4 and -17.9 mWm^{-2} Tg^{-1} for OA, and between -3.6 and -10.3 Wm^{-2} Tg^{-1} for SO_4. The HTAP1 study by Yu et al. (2013), which is based on data from nine CTMs and uses emissions for year 2001 as a baseline, obtained for instance an RF of 27.3 mWm^{-2} Tg^{-1} for BC from emission reductions in the NAM region. This is substantially lower than our 51.9 mWm^{-2} Tg^{-1} for the same case, which is related to the host model used to calculate the AFE: As mentioned in Sect. 2.2., we calculate RF based on the OsloCTM2 model, which ranks among the models with highest AFE for BC in an AeroCom intercomparison study (Myhre et al., 2013). Conversely, GOCART, which was used to calculate the RF in Yu et al. (2013), had the lowest AFE for BC among the investigated AeroCom models. The same AeroCom study found that AFE for SO_4 was much more similar between these two host models, and while we find for NAM an SO_4 RF of -4.5 mWm^{-2} Tg^{-1}, the number from Yu et al. (2013) is a fairly similar -3.9 mWm^{-2} Tg^{-1}. See Samset and Myhre (2015) for a discussion of the AFE in OsloCTM2.

Mitigations in the Middle East give the largest forcing per Tg emission change for all aerosol species. The particularly large BC forcing (201.8 $mWm^{-2}Tg^{-1}$) is probably related to the region's high surface

Atmos. Chem. Phys. Discuss., doi:10.5194/acp-2016-443, 2016
Manuscript under review for journal Atmos. Chem. Phys.
Published: 10 June 2016

albedo, as also found in Samset and Myhre (2015). For OA and SO_4, which are more subject to wet scavenging, the dry atmospheric conditions of the region (Table 2) favor long lifetimes, as shown in Fig. 2 (bottom row).The opposite can be seen in Russia, for which OA and SO_4 forcing is the weakest; here, the lifetime is the shortest among the regions for these species, and the AFE values are the smallest (solid blue lines, Fig. 6). Note that while the annually averaged precipitation amount for 2010 was not particularly high in RBU, the region has a high average cloud cover (Table 2 and Fig. 7), which contributes to wet scavenging. The SAS region also has high RF for all three aerosol species. For BC, this may be related to the region's high convective activity, which promotes long-range aerosol transport and therefore high-altitude MMR changes, which due to the BC AFE profile increases the resulting forcing.

In parentheses in Table 3, we show the relative standard deviation (RSD) values for the RF calculations – i.e. the sample standard deviation divided by the mean – as a representation of inter-model spread. In Yu et al. (2013) inter-model differences were also found to be substantial. One reason was the large variation in emissions used by the models, but the remaining range in AFE values showed that differences between aerosol optical properties, treatment of transport and wet removal, and model native meteorology were still large. Our results, which are based on simulations using the same set of emissions, also shows notable inter-model differences. This underlines the importance of model variations in the various aerosol-related parametrizations – in agreement with previous studies (Textor et al., 2007; Wilcox et al., 2015).

A more detailed perspective of the global forcing averages of Table 3 can be found in Fig. 8, which shows the RF, at top-of-atmosphere, estimated to be exerted due to the aerosol abundance change in each OsloCTM2 model layer. The diversity between models seen in Fig. 4 is naturally still present, but, in particular for BC, the relative importance of low and high altitudes has shifted. The strongly increasing BC AFE with altitude dampens BC variability close to the surface, and emphasizes differences at high altitude. For SO_4, the peak in AFE close to 900hPa coincides with regions of high concentration, leading to increased effective variability in RF exerted close to the surface. For the same reasons, the particularly large upper-level MMR differences between the models for the *SASreduced* experiment (Fig. 4) show enhanced RF for BC but dampened for SO_4.

3.4 Local versus remote impacts of emission mitigation

We move on to quantify how emission mitigations in the six source regions influence radiative forcing both locally within the source region and in other receptor regions. The leftmost column of Fig. 9 shows the effect of domestic emission reductions on local RF from SO_4, OA and BC (Fig. 9 (a), 9 (c) and 9 (e), respectively). To account for the effect of the large variation in baseline emissions between the source regions, we have divided the RF by the annually averaged multi-model median emission change of the source region in question (this gives the forcing efficiency for a given emission change, but to avoid confusion with the aerosol forcing efficiency, or AFE, profiles used to calculate the RF we will refer to this quantity as the emission-weighted forcing). Hence, while e.g. EAS has much larger SO_2 emissions than the other regions (Fig. 2) and therefore much larger absolute local forcing (not shown), the difference in the emission-weighted forcing in Fig. 9a is caused by other factors than the difference in emission levels. For all species, however, the emission-weighted domestic forcings for the SAS and MDE regions stand out as substantially higher than the other regions. The numerical values corresponding to Fig. 9 are presented in Tables S-6 through S-8.

Atmos. Chem. Phys. Discuss., doi:10.5194/acp-2016-443, 2016
Manuscript under review for journal Atmos. Chem. Phys.
Published: 10 June 2016

Notice that Fig. 9 (a), 9 (c) and 9 (e) have two bars per source region – one solid and one dashed. The solid bar shows the emission-weighted forcing calculated by Eq. (1), fully accounting for the vertical aerosol and AFE profile. The hatched bar, however, shows a version calculated by Eq. (2), where we instead use vertically averaged AFE numbers and total column burden changes (equivalent to the method that was used for HTAP1 results in Yu et al. (2013)). We can thus study how accounting for the vertical profiles influences the magnitude of the emission-weighted forcing. For SO_4, the vertically resolved RF calculation gives stronger emission-weighted forcings than the ones using column burdens: averaged across the regions, treating vertical profiles strengthens SO_4 emission-weighted RF by 25 %. The reason for this is that domestic emission reductions cause changes in atmospheric aerosol concentrations primarily at low levels, where AFE for SO_4 is high. For BC, on the other hand, RF is reduced by 37 % when accounting for the vertical dimension, because AFE for BC is weak in the lower atmosphere. For OA, including the vertical information induces only a small increase in emission-weighted RF of about 8 %. This is unsurprising, given the weak altitude dependence of OA AFE as shown in Fig. 6.

The rightmost column of Fig. 9 – Fig. 9 (b), 9 (d) and 9 (f) – shows how emission reductions in different source regions (see x axis) influence the emission-weighted forcing in other receptor regions (indicated by the colors of the bars clustered above each source region). In general, the extra-regional forcing is largest for nearby upwind source regions. For instance, for all aerosol species perturbations in North America have a large effect on the emission-weighted forcing in Europe. Russia, closely followed by Europe, is the region with the largest influence on the Arctic, and Russia and Europe also have a strong influence on each other. We similarly find that South Asia has a very large impact on the emission-weighted forcing in East Asia. However, as noted by Chakraborty et al. (2015) who studied ozone transport between South and East Asia based on HTAP1 simulations, the influence on South Asia on East Asia is limited by the onset of the monsoon season, during which the prevailing wind pattern turns the influence the other way around. In fact, Chakraborty et al. (2015) found that when focusing on the populated parts of these regions, the emission changes over East Asia had a larger impact on populated parts of South Asia than vice versa, due to the specific monthly variations of the meteorological conditions. Another HTAP1 study investigating reductions in methane and ozone precursor emissions found that among the four source regions NAM, EUR, SAS and EAS, the SAS region posed the largest emission-weighted influence in terms of radiative forcing, as this region was located closest to the equator and therefore had the strongest photochemistry, but also due to the strong vertical mixing during the monsoon season (Fry et al., 2012).

While it is useful to compare extra-regional effects per Tg emission reduction, the potential for sizable emission reductions is likely to be lower in the regions with the lowest baseline emissions (Table 2). When we estimated the impact of intercontinental transport by calculating the RERER coefficient (Eq. 3), we therefore use absolute (as opposed to emission-weighted) numbers. Table 4 shows RERER values for all species and regions. For SO_4 burden change, RERER is found to be between 0.32 and 0.76 for the various regions, with values approaching one indicating a larger extra-regional contribution. OA burden RERER ranges from 0.09 to 0.90, while BC burden RERER ranges from 0.18 to 0.87. The RERER values are consistent with Chin et al. (manuscript in preparation), who investigated RERER for HTAP2 data based on surface concentrations. Due to the experiment design, the source regions are not fully identical between HTAP1 and HTAP2, so for easier comparison to HTAP1 studies, a version of Table 4 calculated using the HTAP1 definitions for receptor regions is included in Table S-9. The main features are the same as in Table 4, but the values are in general higher, as expected since the receptor regions are larger for HTAP1 than for HTAP2. This difference is most prominent for Europe.

Atmos. Chem. Phys. Discuss., doi:10.5194/acp-2016-443, 2016
Manuscript under review for journal Atmos. Chem. Phys.
Published: 10 June 2016

To investigate the impact of the vertical distribution of aerosols, we also calculate RERER for RF estimated with the vertically resolved AFE distributions (see bottom half of Table 4.) RERER for SO_4 and OA are broadly similar for burden change and RF. BC RERER, however, is markedly higher (by 30 %, averaged over all source regions) for RF. This is due to long range transport predominantly taking place at high altitudes, where BC AFE is strong. Hence any transported BC will have a higher impact on the RF in remote regions, relative to the source region where it originates close to the ground. For OA and BC, the RERER for the SAS region is the lowest among the regions, which means that a relatively large fraction of emitted aerosol stays within the region. The RBU and MDE regions stand out with very high RERER values, indicating that the regions are very sensitive to extra-regional emission changes. For BC, a high sensitivity of the NAM region to extra-regional emissions is witnessed by a high RERER value. This sensitivity of North America to emission changes in other regions has also been noted in other studies, e.g. in a satellite study by Yu et al. (2012).

To visualize the impact on intercontinental transport on the RF that a given receptor region experiences due to emission reductions in different source regions, we present in Figure 10 a stacked bar plot. For each species and averaged over the different receptor regions (see x axis), the colors show how much a 20% emission reduction in each of the source region contributes to the summed forcing from all source regions, in percent. The summed forcing that the receptor region experiences from the six experiments is given above each bar. This figure illustrates for instance that the main contributor to the high RERER value in the NAM region is EAS: for BC, more than 40 % of the total forcing originates from emission changes in EAS. The HTAP1 study by Yu et al. (2013) also conluded that East Asia posed the largest influence on North America for BC RF. However, they also found that for SO_4 RF, South Asia was strongly influenced by emission changes in Europe. This we do not see in our results, probably because the baseline emissions in Yu et al. (2013) were for approximately the year 2001, for which European SO_4 emissions were substantially higher and Indian emissions lower. Other HTAP1 studies also point to a strong influence of European emission changes: Anenberg et al. (2014) studied impacts of intercontinental transport of fine particulate matter on human mortality, and found that 17 and 13 % of global deaths could be avoided by reducing North American and European emissions, as opposed to 4 and 2 % for South and East Asia. The main reason for this, however, was higher downwind populations for the two first regions as opposed to the two last. Figure 10 shows that domestic mitigations dominate the contribution to the total RF in South and East Asia, and these are also the regions with the largest forcing contributions to other regions. However, it is important to note that this relationship is strongly driven by the fact that the baseline emissions (and hence the 20% emission changes) in EAS and SAS are the largest of all regions, and as we saw from Fig. 9, the relationship changes when looking at emission-weighted numbers: While Fig. 10 shows e.g. a strong contribution from EAS to the forcing in RBU, Fig. 9 demonstrated that per Tg emission reduction EUR has a much stronger influence on RBU than EAS.

4. Summary and Conclusions

We have compared RF for the direct aerosol effect from regional 20 % reductions in anthropogenic aerosol emissions, for ten global climate and chemical transport models participating in the HTAP2 multi-model exercise for the year 2010. We focused on the model experiments simulating emission reductions in North America, Europe, South Asia, East Asia, Russia/Belarussia/Ukraine and the Middle East. We find that the globally averaged TOA radiative forcing exerted per Tg of emission reduction varies between the source regions from 51.9 to 210.8 mWm^{-2} Tg^{-1} for BC, from -2.4 to -17.9

mWm^{-2} Tg^{-1} for OA, and from -3.6 to -10.3 Wm^{-2} Tg^{-1} for SO_4. For all species, the globally averaged emission-weighted forcing from the Middle East was larger than from emission reductions in the other regions, primarily due to the long lifetime of aerosols originating from this region. For BC, the emission-weighted forcing was particularly strong due to the high albedo of the Middle East. The second highest values were caused by emission changes in South Asia, due to the high convective activity and relatively large aerosol lifetime and the low-latitude location. This region, as well as the East Asian region, also induced the largest regionally averaged emission-weighted forcing in a number of investigated receptor regions, especially for BC. Mitigations in Europe have strongest impacts on Russia, the Arctic and the Middle East.

BC emissions in East Asia are found to be more important to North America than domestic mitigation, which is consistent with previous findings pertaining the 2000s. A similar feature was found for Russia for OA and BC; the RF contribution from mitigations in Europe and East Asia outweighs the region's own influence – at least when mitigations are defined as 20% of the region's baseline emissions. For the Middle East, East Asia dominates the RF contribution of OA and BC.

We have also gone beyond previous HTAP studies and investigate the impact of using vertically resolved concentrations of atmospheric aerosols when estimating global mean aerosol radiative forcing and intercontinental transport. Using vertically resolved AFE distributions strengthens SO_4 RF for all regions, relative to using vertically averaged distributions. BC RF weakens when using fully resolved distributions, due to a larger weight being put on BC near sources, close to the ground, where BC AFE is lower. The same feature, only weaker due to a weaker AFE profile, can be observed for OA. While atmospheric transport of SO_4 and OA is only weakly affected, the influence of inter-continental transport to BC forcing is strengthened by 30 % when accounting for the vertical aspect, because long-range transport leads primarily to aerosol changes at high altitudes, where BC AFE is strong.

Acknowledgement:
This work was supported by the Research Council of Norway through the grants AC/BC (240372), NetBC (244141) and SLAC. The CESM project is supported by the National Science Foundation and the Office of Science (BER) of the U. S. Department of Energy. The National Center for Atmospheric Research is funded by the National Science Foundation. The SPRINTARS is supported by the supercomputer system of the National Institute for Environmental Studies, Japan, the Environment Research and Technology Development Fund (S-12-3) of the Ministry of the Environment, Japan, and

JSPS KAKENHI grants 15H01728 and 15K12190. Johannes Flemming's contribution has been supported by the Copernicus Atmosphere Service.

References

Allen, D. J., Pickering, K. E., and Molod, A.: An evaluation of deep convective mixing in the Goddard Chemical Transport Model using International Satellite Cloud Climatology Project cloud parameters, Journal of Geophysical Research: Atmospheres, 102, 25467-25476, 10.1029/97JD02401, 1997.

Anenberg, S. C., West, J. J., Yu, H., Chin, M., Schulz, M., Bergmann, D., Bey, I., Bian, H., Diehl, T., Fiore, A., Hess, P., Marmer, E., Montanaro, V., Park, R., Shindell, D., Takemura, T., and Dentener, F.: Impacts of intercontinental transport of anthropogenic fine particulate matter on human mortality, Air Quality, Atmosphere & Health, 7, 369-379, 10.1007/s11869-014-0248-9, 2014.

Ban-Weiss, G. A., Cao, L., Bala, G., and Caldeira, K.: Dependence of climate forcing and response on the altitude of black carbon aerosols, Climate Dynamics, 38, 897-911, 10.1007/s00382-011-1052-y, 2011.

Berntsen, T., Fuglestvedt, J., Myhre, G., Stordal, F., and Berglen, T. F.: Abatement of greenhouse gases: Does location matter?, Climatic Change, 74, 377-411, 2006.

Bian, H., Chin, M., Rodriguez, J. M., Yu, H., Penner, J. E., and Strahan, S.: Sensitivity of aerosol optical thickness and aerosol direct radiative effect to relative humidity, Atmos Chem Phys, 9, 2375-2386, 2009.

Bollasina, M. A., Ming, Y., and Ramaswamy, V.: Anthropogenic Aerosols and the Weakening of the South Asian Summer Monsoon, Science, 334, 502-505, 10.1126/science.1204994, 2011.

Boucher, O., Randall, D., Artaxo, P., Bretherton, C., Feingold, G., Forster, P., Kerminen, V.-M., Kondo, Y., Liao, H., Lohmann, U., Rasch, P., Satheesh, S. K., Sherwood, S., Stevens, B., and Zhang, X. Y.: Clouds and Aerosols. In: Climate Change 2013: The Physical Science Basis. Contribution of Working Group I to the Fifth Assessment Report of the Intergovernmental Panel on Climate Change [Stocker, T.F., D. Qin, G.-K. Plattner, M. Tignor, S.K. Allen, J. Boschung, A. Nauels, Y. Xia, V. Bex and P.M. Midgley (eds.)], Cambridge University Press, Cambridge, United Kingdom and New York, NY, USA., 2013.

Brauer, M., Freedman, G., Frostad, J., van Donkelaar, A., Martin, R. V., Dentener, F., Dingenen, R. v., Estep, K., Amini, H., Apte, J. S., Balakrishnan, K., Barregard, L., Broday, D., Feigin, V., Ghosh, S., Hopke, P. K., Knibbs, L. D., Kokubo, Y., Liu, Y., Ma, S., Morawska, L., Sangrador, J. L. T., Shaddick, G., Anderson, H. R., Vos, T., Forouzanfar, M. H., Burnett, R. T., and Cohen, A.: Ambient Air Pollution Exposure Estimation for the Global Burden of Disease 2013, Environmental Science & Technology, 50, 79-88, 10.1021/acs.est.5b03709, 2016.

Chakraborty, T., Beig, G., Dentener, F. J., and Wild, O.: Atmospheric transport of ozone between Southern and Eastern Asia, Science of The Total Environment, 523, 28-39, http://dx.doi.org/10.1016/j.scitotenv.2015.03.066, 2015.

Chikira, M., and Sugiyama, M.: A Cumulus Parameterization with State-Dependent Entrainment Rate. Part I: Description and Sensitivity to Temperature and Humidity Profiles, Journal of the Atmospheric Sciences, 67, 2171-2193, 10.1175/2010JAS3316.1, 2010.

Chin, M., Rood, R. B., Lin, S.-J., Müller, J.-F., and Thompson, A. M.: Atmospheric sulfur cycle simulated in the global model GOCART: Model description and global properties, Journal of Geophysical Research: Atmospheres, 105, 24671-24687, 10.1029/2000JD900384, 2000.

Colarco, P., da Silva, A., Chin, M., and Diehl, T.: Online simulations of global aerosol distributions in the NASA GEOS-4 model and comparisons to satellite and ground-based aerosol optical depth, Journal of Geophysical Research: Atmospheres, 115, n/a-n/a, 10.1029/2009JD012820, 2010.

Fierz-Schmidhauser, R., Zieger, P., Wehrle, G., Jefferson, A., Ogren, J. A., Baltensperger, U., and Weingartner, E.: Measurement of relative humidity dependent light scattering of aerosols, Atmos. Meas. Tech., 3, 39-50, 10.5194/amt-3-39-2010, 2010.

Flemming, J., Huijnen, V., Arteta, J., Bechtold, P., Beljaars, A., Blechschmidt, A. M., Diamantakis, M., Engelen, R. J., Gaudel, A., Inness, A., Jones, L., Josse, B., Katragkou, E., Marecal, V., Peuch, V. H., Richter, A., Schultz, M. G., Stein, O., and Tsikerdekis, A.: Tropospheric chemistry in the Integrated Forecasting System of ECMWF, Geosci. Model Dev., 8, 975-1003, 10.5194/gmd-8-975-2015, 2015.

Fry, M. M., Naik, V., West, J. J., Schwarzkopf, M. D., Fiore, A. M., Collins, W. J., Dentener, F. J., Shindell, D. T., Atherton, C., Bergmann, D., Duncan, B. N., Hess, P., MacKenzie, I. A., Marmer, E., Schultz, M. G., Szopa, S., Wild, O., and Zeng, G.: The influence of ozone precursor emissions from four world regions on tropospheric composition and radiative climate forcing, Journal of Geophysical Research: Atmospheres, 117, n/a-n/a, 10.1029/2011JD017134, 2012.

Geng, F. H., Hua, J., Mu, Z., Peng, L., Xu, X. H., Chen, R. J., and Kan, H. D.: Differentiating the associations of black carbon and fine particle with daily mortality in a Chinese city, Environ Res, 120, 27-32, 2013.

Hack, J. J., Caron, J. M., Yeager, S. G., Oleson, K. W., Holland, M. M., Truesdale, J. E., and Rasch, P. J.: Simulation of the Global Hydrological Cycle in the CCSM Community Atmosphere Model Version 3 (CAM3): Mean Features, Journal of Climate, 19, 2199-2221, 10.1175/JCLI3755.1, 2006.

Haywood, J. M., Ramaswamy, V., and Donner, L. J.: A limited-area-model case study of the effects of sub-grid scale Variations in relative humidity and cloud upon the direct radiative forcing of sulfate aerosol, Geophys Res Lett, 24, 143-146, 10.1029/96gl03812, 1997.

Haywood, J. M., and Shine, K. P.: Multi-spectral calculations of the direct radiative forcing of tropospheric sulphate and soot aerosols using a column model, Quarterly Journal of the Royal Meteorological Society, 123, 1907-1930, 10.1002/qj.49712354307, 1997.

Henze, D. K., Hakami, A., and Seinfeld, J. H.: Development of the adjoint of GEOS-Chem, Atmos. Chem. Phys., 7, 2413-2433, 10.5194/acp-7-2413-2007, 2007.

HTAP: Hemispheric Transport of Air Pollution, Part A: Ozone and particulate matter, Geneva, Switzerland, 2010.

Huang, J., Minnis, P., Chen, B., Huang, Z., Liu, Z., Zhao, Q., Yi, Y., and Ayers, J. K.: Long-range transport and vertical structure of Asian dust from CALIPSO and surface measurements during PACDEX, Journal of Geophysical Research: Atmospheres, 113, n/a-n/a, 10.1029/2008JD010620, 2008.

Janssen, N. A. H. e. a.: Health Effects of Black Carbon World Health Organization, 2012.

Janssens-Maenhout, G., Crippa, M., Guizzardi, D., Dentener, F., Muntean, M., Pouliot, G., Keating, T., Zhang, Q., Kurokawa, J., Wankmüller, R., Denier van der Gon, H., Kuenen, J. J. P., Klimont, Z., Frost,

G., Darras, S., Koffi, B., and Li, M.: HTAP_v2.2: a mosaic of regional and global emission grid maps for 2008 and 2010 to study hemispheric transport of air pollution, Atmos. Chem. Phys., 15, 11411-11432, 10.5194/acp-15-11411-2015, 2015.

Khain, A. P.: Notes on state-of-the-art investigations of aerosol effects on precipitation: a critical review, Environmental Research Letters, 4, 015004, 2009.

Kipling, Z., Stier, P., Johnson, C. E., Mann, G. W., Bellouin, N., Bauer, S. E., Bergman, T., Chin, M., Diehl, T., Ghan, S. J., Iversen, T., Kirkevåg, A., Kokkola, H., Liu, X., Luo, G., van Noije, T., Pringle, K. J., von Salzen, K., Schulz, M., Seland, Ø., Skeie, R. B., Takemura, T., Tsigaridis, K., and Zhang, K.: What controls the vertical distribution of aerosol? Relationships between process sensitivity in HadGEM3–UKCA and inter-model variation from AeroCom Phase II, Atmos. Chem. Phys. Discuss., 15, 25933-25980, 10.5194/acpd-15-25933-2015, 2015.

Koch, D., and Del Genio, A. D.: Black carbon semi-direct effects on cloud cover: review and synthesis, Atmos. Chem. Phys., 10, 7685-7696, 10.5194/acp-10-7685-2010, 2010.

Koffi, B. D., F.; Keating, T.; Galmarini, S.; Hogrefe, C.; Schulz, M.; Manhout-Janssens, G.: Harmonization of the multi-scale multi-model activity HTAP, AQMEII and MICS ASIA: simulations set ups, emission inventory variables, boundary conditions and output formats, To be submitted to Atmos. Chem. Phys., 2016.

Liu, B., Xu, M., and Henderson, M.: Where have all the showers gone? Regional declines in light precipitation events in China, 1960–2000, International Journal of Climatology, 31, 1177-1191, 10.1002/joc.2144, 2011.

Liu, D., Wang, Z., Liu, Z., Winker, D., and Trepte, C.: A height resolved global view of dust aerosols from the first year CALIPSO lidar measurements, Journal of Geophysical Research: Atmospheres, 113, n/a-n/a, 10.1029/2007JD009776, 2008.

Lohmann, U., and Feichter, J.: Global indirect aerosol effects: a review, Atmos. Chem. Phys., 5, 715-737, 10.5194/acp-5-715-2005, 2005.

Molod, A., Takacs, L., Suarez, M., and Bacmeister, J.: Development of the GEOS-5 atmospheric general circulation model: evolution from MERRA to MERRA2, Geosci. Model Dev., 8, 1339-1356, 10.5194/gmd-8-1339-2015, 2015.

Moorthi, S., and Suarez, M. J.: Relaxed Arakawa-Schubert. A Parameterization of Moist Convection for General Circulation Models, Monthly Weather Review, 120, 978-1002, 10.1175/1520-0493(1992)120<0978:RASAPO>2.0.CO;2, 1992.

Myhre, G., Stordal, F., Berglen, T., Sundet, J. K., and Isaksen, I. S. A.: Uncertainties in the Radiative Forcing Due to Sulfate Aerosols, J Atmos Sci, 2004.

Myhre, G., Samset, B. H., Schulz, M., Balkanski, Y., Bauer, S., Berntsen, T. K., Bian, H., Bellouin, N., Chin, M., Diehl, T., Easter, R. C., Feichter, J., Ghan, S. J., Hauglustaine, D., Iversen, T., Kinne, S., Kirkevåg, A., Lamarque, J. F., Lin, G., Liu, X., Lund, M. T., Luo, G., Ma, X., van Noije, T., Penner, J. E., Rasch, P. J., Ruiz, A., Seland, Ø., Skeie, R. B., Stier, P., Takemura, T., Tsigaridis, K., Wang, P., Wang, Z., Xu, L., Yu, H., Yu, F., Yoon, J. H., Zhang, K., Zhang, H., and Zhou, C.: Radiative forcing of the direct aerosol effect from AeroCom Phase II simulations, Atmos. Chem. Phys., 13, 1853-1877, 10.5194/acp-13-1853-2013, 2013.

Myhre, G., and Samset, B. H.: Standard climate models radiation codes underestimate black carbon radiative forcing, Atmos. Chem. Phys., 15, 2883-2888, 10.5194/acp-15-2883-2015, 2015.

Rienecker, M. M., Suarez, M. J., Todling, R., Bacmeister, J., Takacs, L., Liu, H.-C., Gu, W., Sienkiewicz, M., Koster, R. D., Gelaro, R., Stajner, I., and Nielsen, J. E.: The GEOS-5 Data Assimilation System — Documentation of Versions 5.0.1, 5.1.0, and 5.2.0, NASA, 2008.

Samset, B. H., and Myhre, G.: Vertical dependence of black carbon, sulphate and biomass burning aerosol radiative forcing, Geophysical Research Letters, 38, n/a-n/a, 10.1029/2011GL049697, 2011.

Samset, B. H., Myhre, G., Schulz, M., Balkanski, Y., Bauer, S., Berntsen, T., Bian, H., Bellouin, N., Diehl, T., Easter, R. C., Ghan, S. J., Iversen, T., Kinne, S., Kirkevåg, A., Lamarque, J. F., Lin, G., Liu, X., Penner, J. E., Seland, Ø., Skeie, R. B., Stier, P., Takemura, T., Tsigaridis, K., and Zhang, K.: Black carbon vertical profiles strongly affect its radiative forcing uncertainty, Atmos. Chem. Phys., 13, 2423-2434, 10.5194/acp-13-2423-2013, 2013.

Samset, B. H., Myhre, G., Herber, A., Kondo, Y., Li, S. M., Moteki, N., Koike, M., Oshima, N., Schwarz, J. P., Balkanski, Y., Bauer, S. E., Bellouin, N., Berntsen, T. K., Bian, H., Chin, M., Diehl, T., Easter, R. C., Ghan, S. J., Iversen, T., Kirkevåg, A., Lamarque, J. F., Lin, G., Liu, X., Penner, J. E., Schulz, M., Seland, Ø., Skeie, R. B., Stier, P., Takemura, T., Tsigaridis, K., and Zhang, K.: Modelled black carbon radiative forcing and atmospheric lifetime in AeroCom Phase II constrained by aircraft observations, Atmos. Chem. Phys., 14, 12465-12477, 10.5194/acp-14-12465-2014, 2014.

Samset, B. H., and Myhre, G.: Climate response to externally mixed black carbon as a function of altitude, Journal of Geophysical Research: Atmospheres, 120, 2014JD022849, 10.1002/2014JD022849, 2015.

Shindell, D., Kuylenstierna, J. C. I., Vignati, E., van Dingenen, R., Amann, M., Klimont, Z., Anenberg, S. C., Muller, N., Janssens-Maenhout, G., Raes, F., Schwartz, J., Faluvegi, G., Pozzoli, L., Kupiainen, K., Hoglund-Isaksson, L., Emberson, L., Streets, D., Ramanathan, V., Hicks, K., Oanh, N. T. K., Milly, G., Williams, M., Demkine, V., and Fowler, D.: Simultaneously Mitigating Near-Term Climate Change and Improving Human Health and Food Security, Science, 335, 183-189, DOI 10.1126/science.1210026, 2012.

Simpson, D., Benedictow, A., Berge, H., Bergström, R., Emberson, L. D., Fagerli, H., Flechard, C. R., Hayman, G. D., Gauss, M., Jonson, J. E., Jenkin, M. E., Nyíri, A., Richter, C., Semeena, V. S., Tsyro, S., Tuovinen, J. P., Valdebenito, Á., and Wind, P.: The EMEP MSC-W chemical transport model – technical description, Atmos. Chem. Phys., 12, 7825-7865, 10.5194/acp-12-7825-2012, 2012.

Stamnes, K., Tsay, S. C., Wiscombe, W., and Jayaweera, K.: Numerically Stable Algorithm for Discrete-Ordinate-Method Radiative-Transfer in Multiple-Scattering and Emitting Layered Media, Appl Optics, 27, 2502-2509, 1988.

Stevens, B., and Feingold, G.: Untangling aerosol effects on clouds and precipitation in a buffered system, Nature, 461, 607-613, 2009.

Sudo, K., Takahashi, M., Kurokawa, J.-i., and Akimoto, H.: CHASER: A global chemical model of the troposphere 1. Model description, Journal of Geophysical Research: Atmospheres, 107, ACH 7-1-ACH 7-20, 10.1029/2001JD001113, 2002.

Søvde, O. A., Prather, M. J., Isaksen, I. S. A., Berntsen, T. K., Stordal, F., Zhu, X., Holmes, C. D., and Hsu, J.: The chemical transport model Oslo CTM3, Geosci. Model Dev., 5, 1441-1469, 10.5194/gmd-5-1441-2012, 2012.

Takemura, T., Nozawa, T., Emori, S., Nakajima, T. Y., and Nakajima, T.: Simulation of climate response to aerosol direct and indirect effects with aerosol transport-radiation model, Journal of Geophysical Research: Atmospheres, 110, n/a-n/a, 10.1029/2004JD005029, 2005.

Textor, C., Schulz, M., Guibert, S., Kinne, S., Balkanski, Y., Bauer, S., Berntsen, T., Berglen, T., Boucher, O., Chin, M., Dentener, F., Diehl, T., Feichter, J., Fillmore, D., Ginoux, P., Gong, S., Grini, A., Hendricks, J., Horowitz, L., Huang, P., Isaksen, I. S. A., Iversen, T., Kloster, S., Koch, D., Kirkevåg, A., Kristjansson, J. E., Krol, M., Lauer, A., Lamarque, J. F., Liu, X., Montanaro, V., Myhre, G., Penner, J. E., Pitari, G., Reddy, M. S., Seland, Ø., Stier, P., Takemura, T., and Tie, X.: The effect of harmonized emissions on aerosol properties in global models – an AeroCom experiment, Atmos. Chem. Phys., 7, 4489-4501, 10.5194/acp-7-4489-2007, 2007.

Tiedtke, M.: A Comprehensive Mass Flux Scheme for Cumulus Parameterization in Large-Scale Models, Monthly Weather Review, 117, 1779-1800, 10.1175/1520-0493(1989)117<1779:ACMFSF>2.0.CO;2, 1989.

Tilmes, S. L., J.-F.; Emmons, L.K.; Kinnison, D.E.; Marsh, D.; Garcia, R.R.; Smith, A.K.; Neely, R.R.; Conley, A.; Vitt, F.; Val Martin, M.; Tanimoto, H.; Simpson, I.; Blake, D.R.; Blake, N.: Representation of the Community Earth System Model (CESM1) CAM4-chem within the Chemistry-ClimateModel Initiative (CCMI), Accepted for publication in Geosci. Model Dev., 2016, 1-50, 10.5194/gmd-2015-237, 2016.

Tsigaridis, K., Daskalakis, N., Kanakidou, M., Adams, P. J., Artaxo, P., Bahadur, R., Balkanski, Y., Bauer, S. E., Bellouin, N., Benedetti, A., Bergman, T., Berntsen, T. K., Beukes, J. P., Bian, H., Carslaw, K. S., Chin, M., Curci, G., Diehl, T., Easter, R. C., Ghan, S. J., Gong, S. L., Hodzic, A., Hoyle, C. R., Iversen, T., Jathar, S., Jimenez, J. L., Kaiser, J. W., Kirkevåg, A., Koch, D., Kokkola, H., Lee, Y. H., Lin, G., Liu, X., Luo, G., Ma, X., Mann, G. W., Mihalopoulos, N., Morcrette, J. J., Müller, J. F., Myhre, G., Myriokefalitakis, S., Ng, N. L., O'Donnell, D., Penner, J. E., Pozzoli, L., Pringle, K. J., Russell, L. M., Schulz, M., Sciare, J., Seland, Ø., Shindell, D. T., Sillman, S., Skeie, R. B., Spracklen, D., Stavrakou, T., Steenrod, S. D., Takemura, T., Tiitta, P., Tilmes, S., Tost, H., van Noije, T., van Zyl, P. G., von Salzen, K., Yu, F., Wang, Z., Wang, Z., Zaveri, R. A., Zhang, H., Zhang, K., Zhang, Q., and Zhang, X.: The AeroCom evaluation and intercomparison of organic aerosol in global models, Atmos. Chem. Phys., 14, 10845-10895, 10.5194/acp-14-10845-2014, 2014.

Vuolo, M. R., Schulz, M., Balkanski, Y., and Takemura, T.: A new method for evaluating the impact of vertical distribution on aerosol radiative forcing in general circulation models, Atmos. Chem. Phys., 14, 877-897, 10.5194/acp-14-877-2014, 2014.

Watanabe, M., Suzuki, T., O'ishi, R., Komuro, Y., Watanabe, S., Emori, S., Takemura, T., Chikira, M., Ogura, T., Sekiguchi, M., Takata, K., Yamazaki, D., Yokohata, T., Nozawa, T., Hasumi, H., Tatebe, H., and Kimoto, M.: Improved Climate Simulation by MIROC5: Mean States, Variability, and Climate Sensitivity, Journal of Climate, 23, 6312-6335, 10.1175/2010JCLI3679.1, 2010.

Wilcox, L. J., Highwood, E. J., Booth, B. B. B., and Carslaw, K. S.: Quantifying sources of inter-model diversity in the cloud albedo effect, Geophysical Research Letters, 42, 1568-1575, 10.1002/2015GL063301, 2015.

Wu, S., Mickley, L. J., Jacob, D. J., Logan, J. A., Yantosca, R. M., and Rind, D.: Why are there large differences between models in global budgets of tropospheric ozone?, Journal of Geophysical Research: Atmospheres, 112, n/a-n/a, 10.1029/2006JD007801, 2007.

Yu, H., Kaufman, Y. J., Chin, M., Feingold, G., Remer, L. A., Anderson, T. L., Balkanski, Y., Bellouin, N., Boucher, O., Christopher, S., DeCola, P., Kahn, R., Koch, D., Loeb, N., Reddy, M. S., Schulz, M.,

Takemura, T., and Zhou, M.: A review of measurement-based assessments of the aerosol direct radiative effect and forcing, Atmos. Chem. Phys., 6, 613-666, 10.5194/acp-6-613-2006, 2006.

Yu, H., Remer, L. A., Chin, M., Bian, H., Tan, Q., Yuan, T., and Zhang, Y.: Aerosols from Overseas Rival Domestic Emissions over North America, Science, 337, 566-569, 10.1126/science.1217576, 2012.

Yu, H. B., Chin, M., West, J. J., Atherton, C. S., Bellouin, N., Bergmann, D., Bey, I., Bian, H. S., Diehl, T., Forberth, G., Hess, P., Schulz, M., Shindell, D., Takemura, T., and Tan, Q.: A multimodel assessment of the influence of regional anthropogenic emission reductions on aerosol direct radiative forcing and the role of intercontinental transport, Journal of Geophysical Research-Atmospheres, 118, 700-720, 2013.

Zarzycki, C. M., and Bond, T. C.: How much can the vertical distribution of black carbon affect its global direct radiative forcing?, Geophysical Research Letters, 37, n/a-n/a, 10.1029/2010GL044555, 2010.

Zhang, G. J., and McFarlane, N. A.: Sensitivity of climate simulations to the parameterization of cumulus convection in the Canadian climate centre general circulation model, Atmosphere-Ocean, 33, 407-446, 1995.

Zhang, K., Wan, H., Liu, X., Ghan, S. J., Kooperman, G. J., Ma, P. L., Rasch, P. J., Neubauer, D., and Lohmann, U.: Technical Note: On the use of nudging for aerosol–climate model intercomparison studies, Atmos. Chem. Phys., 14, 8631-8645, 10.5194/acp-14-8631-2014, 2014.

Atmos. Chem. Phys. Discuss., doi:10.5194/acp-2016-443, 2016
Manuscript under review for journal Atmos. Chem. Phys.
Published: 10 June 2016

Figures

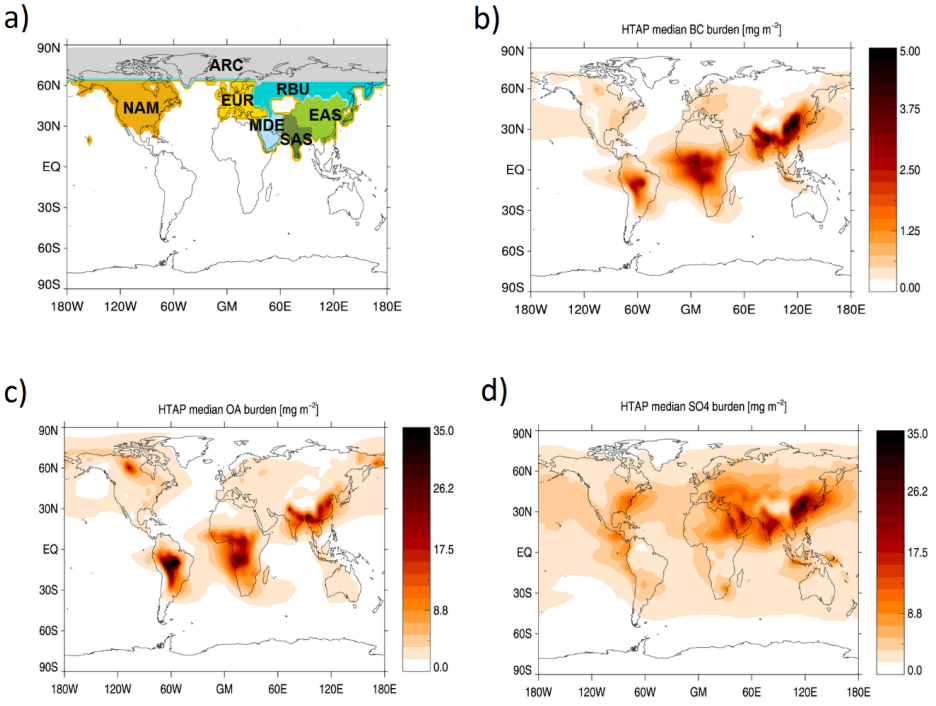

Figure 1: a) Regions of focus (NAM: North America; EUR: Europe; EAS: East Asia; SAS: South Asia; RBU; Russia/Belarussia/Ukraine, MDE: Middle East and ARC: Arctic). b), c) and d) show multi-model median, annual mean aerosol load of the base experiment for BC, OA and SO_4, respectively.

Atmos. Chem. Phys. Discuss., doi:10.5194/acp-2016-443, 2016
Manuscript under review for journal Atmos. Chem. Phys.
Published: 10 June 2016

Atmospheric Chemistry and Physics Discussions

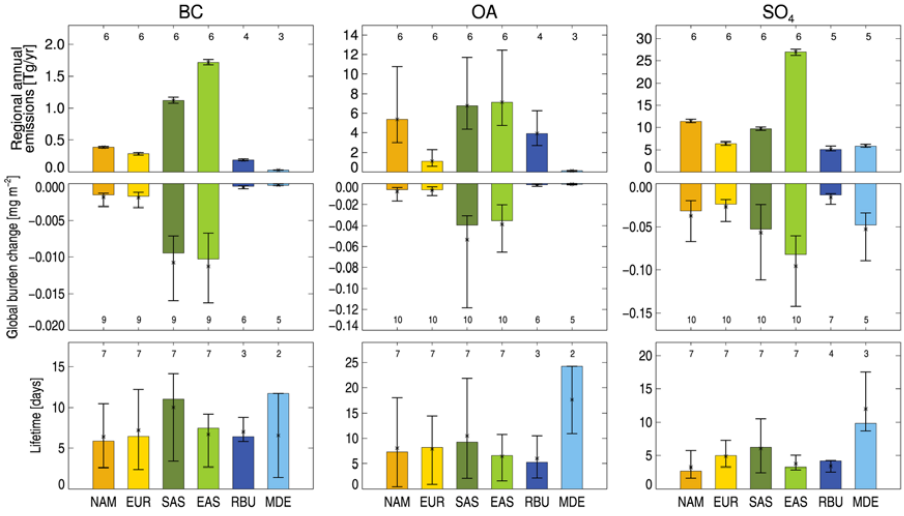

Figure 2: Top row: Regionally averaged annual mean aerosol emissions (for SO_4, we give SO_2 emissions), for the source regions shown in Fig. 1. Numbers are from the *BASE* simulations. Error bars show the maximum and minimum emissions for the sample of models used here, and the numbers above the bars give the number of models that have data for the given value. Middle row: Globally and annually averaged aerosol burden change for 20 % emission reductions in the indicated region. Numbers are from the perturbation simulations. Bottom row: Aerosol lifetime, here defined as the global change in burden divided by the global change in emissions following an emission reduction within a given source region (see main text, Eq. 4).

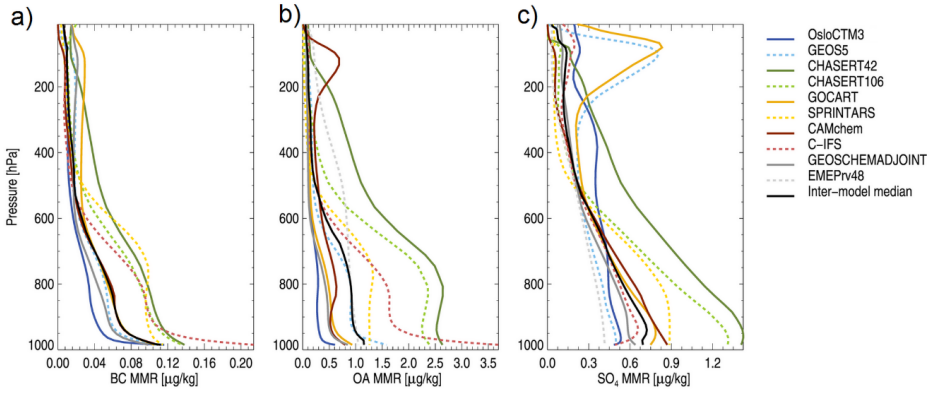

Figure 3: Globally and annually averaged mass mixing ratios (MMR) of a) BC, b) OA and c) SO_4, for all contributing models.

Atmos. Chem. Phys. Discuss., doi:10.5194/acp-2016-443, 2016
Manuscript under review for journal Atmos. Chem. Phys.
Published: 10 June 2016

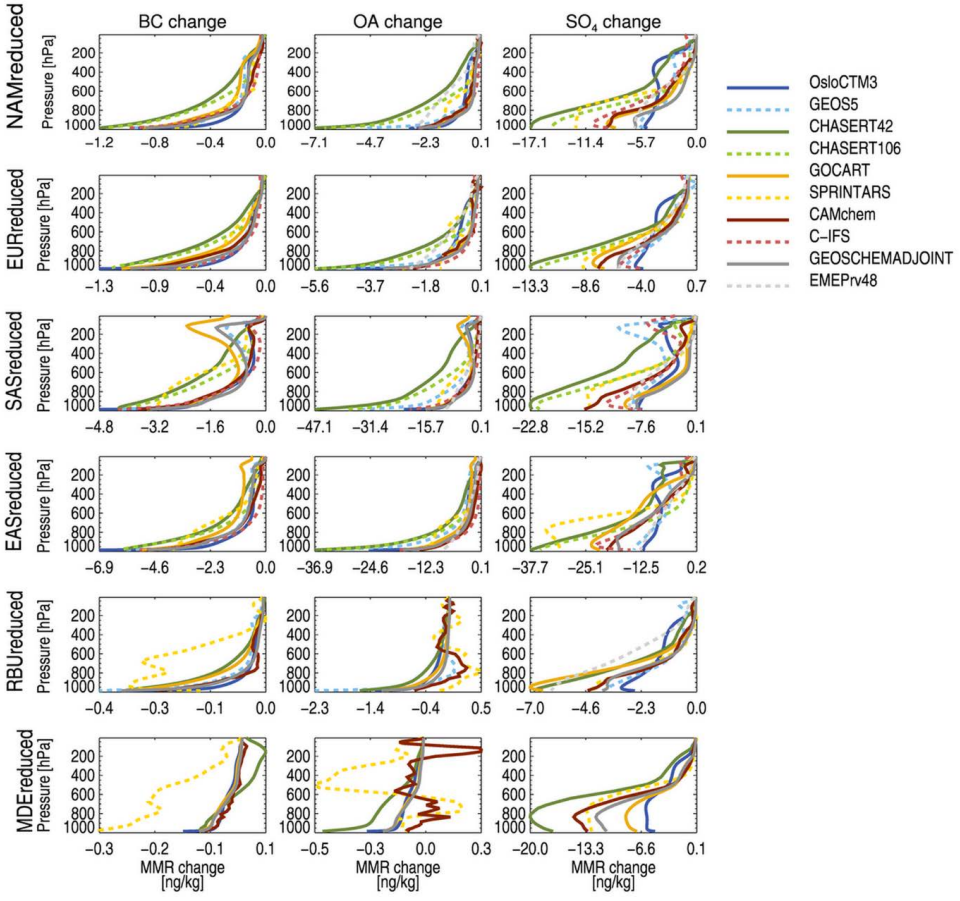

Figure 4: Globally averaged change in MMR per model layer, when reducing emissions by 20 % within the region indicated (rows), for all aerosol species (columns). Each line represents one model. See Tables S-2 to S-4 for the total burden changes for all models, experiments and species.

Atmos. Chem. Phys. Discuss., doi:10.5194/acp-2016-443, 2016
Manuscript under review for journal Atmos. Chem. Phys.
Published: 10 June 2016

Atmospheric Chemistry and Physics
Discussions

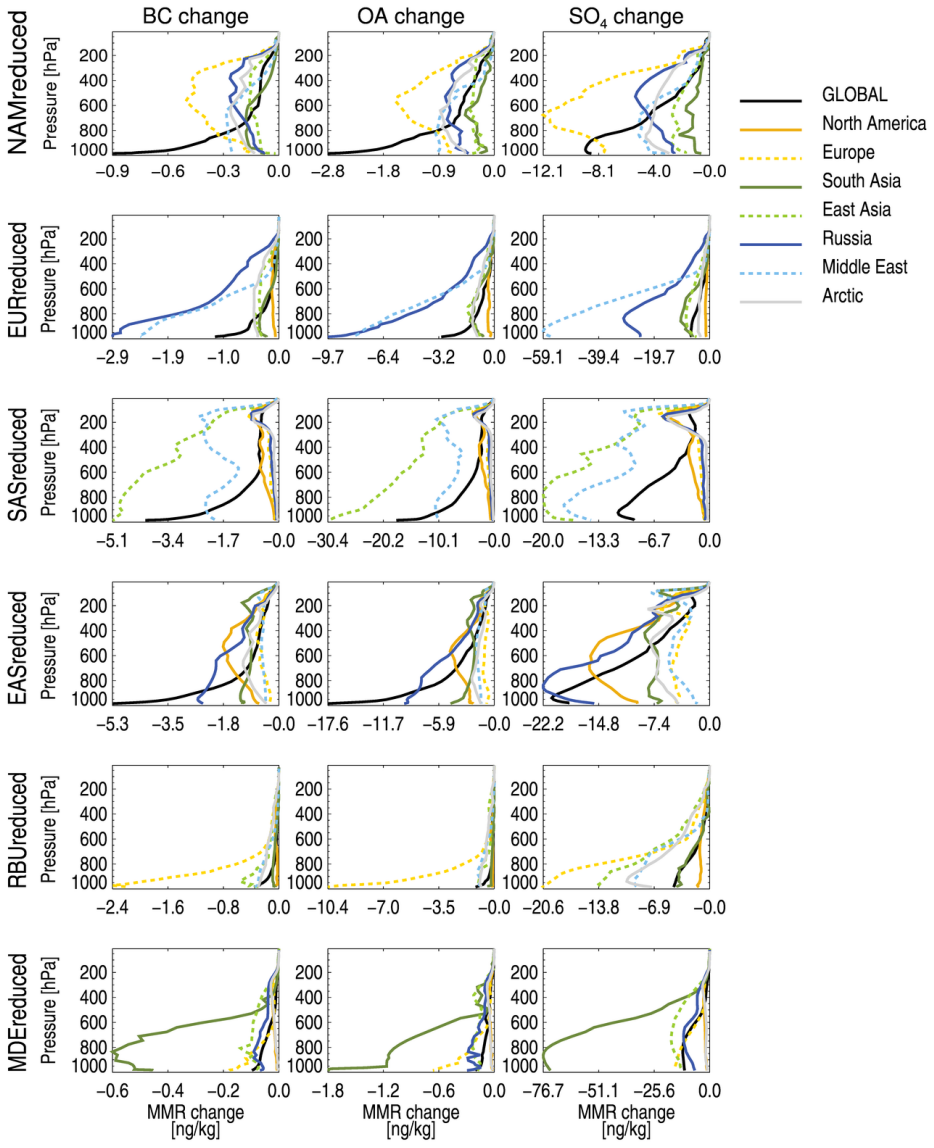

Figure 5: Model-averaged aerosol MMR change profiles for different receptor regions (marked by the colors of the lines), for emission reductions in the six source regions (rows) and for BC (first column), OA (middle column) and SO_4 (last column).

Atmos. Chem. Phys. Discuss., doi:10.5194/acp-2016-443, 2016
Manuscript under review for journal Atmos. Chem. Phys.
Published: 10 June 2016

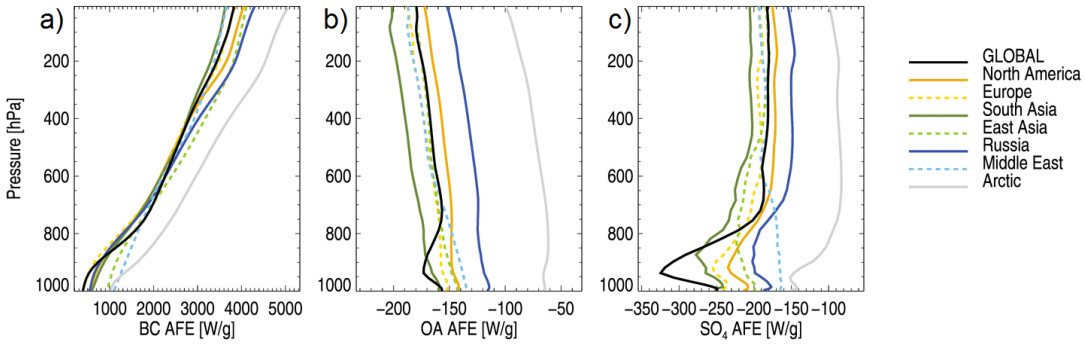

Figure 6: Aerosol forcing efficiency profiles, i.e. TOA radiative forcing exerted per gram of aerosol versus altitude. Black, solid lines indicate global, annual mean profiles. Colored lines show the annual mean profiles within the regions of Figure 1a.

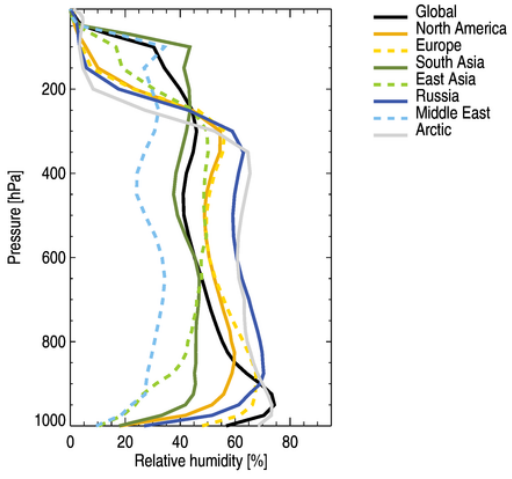

Figure 7: Annually averaged relative humidity from MERRA data, for year 2010, for the same regions as in Figure 6.

Atmos. Chem. Phys. Discuss., doi:10.5194/acp-2016-443, 2016
Manuscript under review for journal Atmos. Chem. Phys.
Published: 10 June 2016

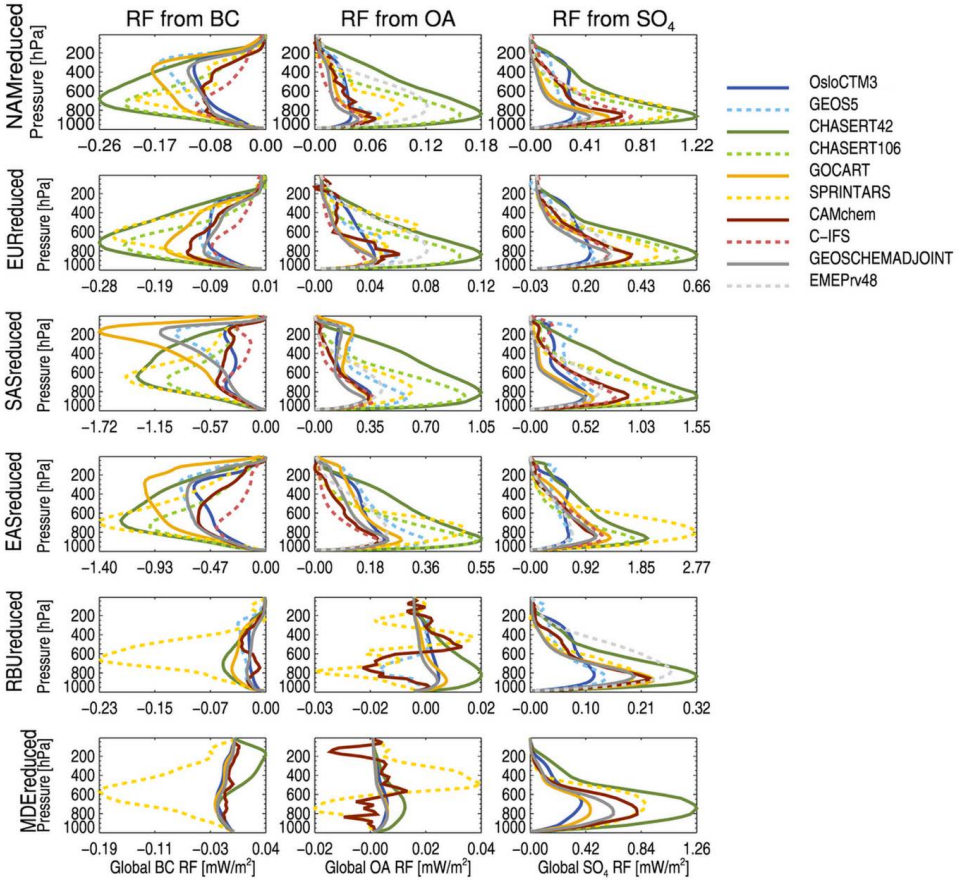

Figure 8: Global mean vertically resolved aerosol direct radiative forcing, when reducing emissions by 20 % within the region indicated (rows), for all aerosol species (columns). Each line represents one model. See Tables S-2 to S-4 for individual model results.

Atmos. Chem. Phys. Discuss., doi:10.5194/acp-2016-443, 2016
Manuscript under review for journal Atmos. Chem. Phys.
Published: 10 June 2016

Atmospheric Chemistry and Physics
Discussions

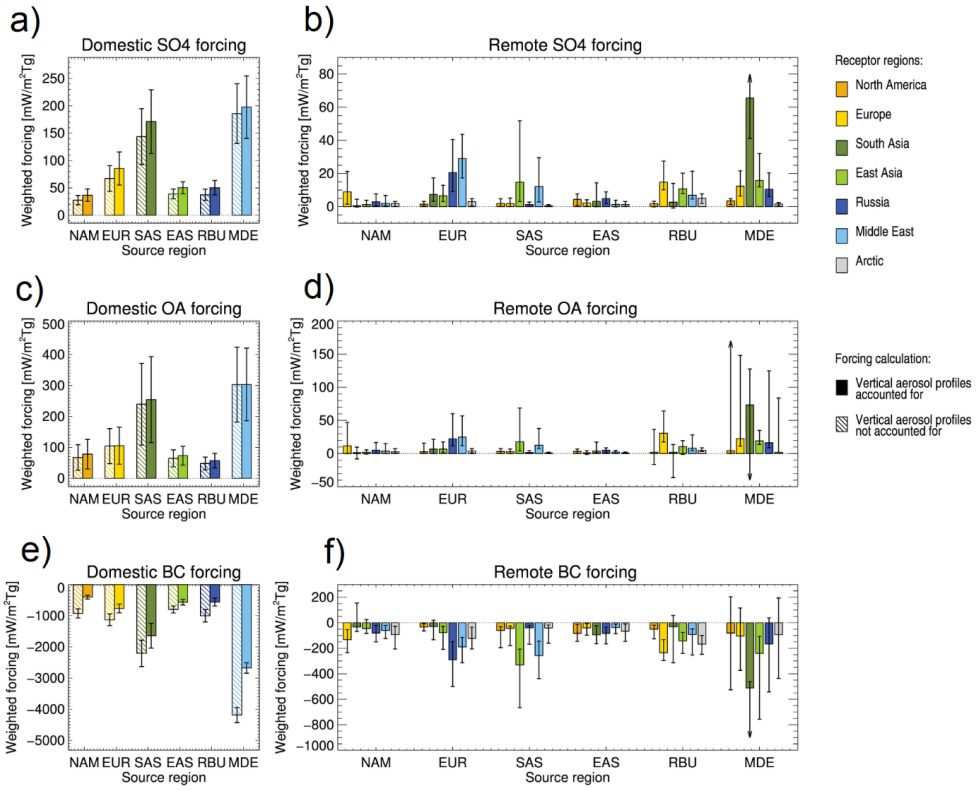

Figure 9: Regionally averaged forcing in the source regions due to domestic emission reductions (leftmost column) and remote forcings in different receptor regions due to emission reductions in the six source regions (rightmost column) for the three aerosol species (tow row: SO_4; middle row: OA; lower row: BC). Forcings are weighed by the emission change in each given source region. The source region in question is marked on the x axis, while the receptor region for which the forcing is averaged is marked by the color of the bar. See Tables S-6 through S-8 for the numbers behind this figure.

Atmos. Chem. Phys. Discuss., doi:10.5194/acp-2016-443, 2016
Manuscript under review for journal Atmos. Chem. Phys.
Published: 10 June 2016

Atmospheric Chemistry and Physics
Discussions

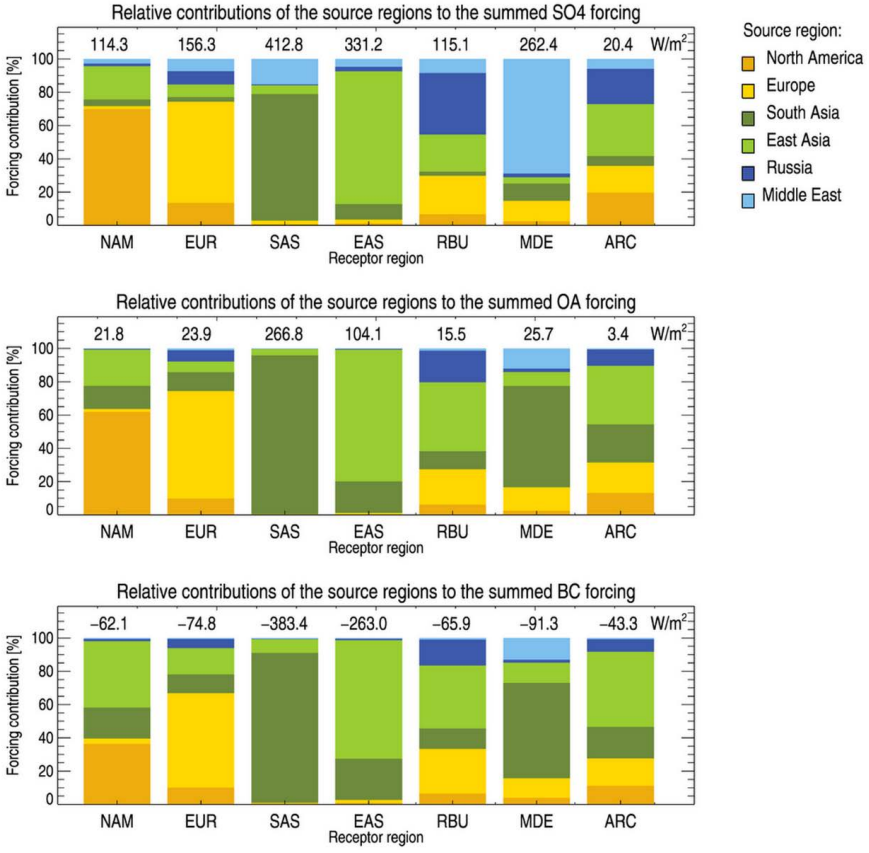

Figure 10: Relative contributions of the individual source regions (colors on the bars) to the summed forcing, averaged over each of the receptor regions (given on the x axis and seen in Fig. 1 (a)). The summed forcing that the given receptor region experiences due to emission-reductions in the six source regions is given in numbers above each bar.

Atmos. Chem. Phys. Discuss., doi:10.5194/acp-2016-443, 2016
Manuscript under review for journal Atmos. Chem. Phys.
Published: 10 June 2016

Atmospheric Chemistry and Physics Discussions

Tables

Table 1: Models used for the present study, with relevant information and references.

	Version	Horizontal resolution	Vert. layers	Meteorology input source	Convection	Reference
SPRINTARS	atmosphere: MIROC5.2	1.1° x 1.1°	56	ECMWF Interim.	The cumulus scheme (Chikira and Sugiyama, 2010) is an entraining plume model, in which the lateral entrainment rate varies vertically depending on the surrounding environment. The cloud base mass flux is determined with a prognostic convective kinetic energy closure.	Watanabe et al. (2010) Takemura et al. (2005)
OsloCTM3	all aerosol modules from OsloCTM2	2.8° x 2.8°	60	ECMWF's Integrated Forecast System (IFS) model	The parameterization of deep convection is based on the Tiedke mass flux scheme (Tiedtke, 1989).	Søvde et al. (2012)
GOCART	v5 2010	1.3° x 1.0°	72	MERRA	Moist convection is parameterized using archived cloud mass flux fields from MERRA. GCTM convection is parameterized using cloud mass flux information from the relaxed Arakawa-Schubert (RAS) algorithm (Moorthi and Suarez, 1992).	Chin et al. (2000)
C-IFS	IFS CY40r2	0.7° x 0.7°	54	Relaxed to ERA-Interim	Tiedtke (1989) shallow convection scheme.	Flemming et al. (2015)
CHASER-T42	v4.0, MIROC-ESM version	2.8° x 2.8°	32	ERA-Interim (u,v,T) and HadISST	Transport due to advection, convection, and other subgrid-scale mixing are simulated "on-line" by the dynamical component of the CCSR/NIES AGCM. The prognostic Arakawa-Schubert scheme is employed to simulate cumulus convection.	Sudo et al. (2002)
CHASER-T106	v4.0, MIROC-ESM version	1.1° x 1.1°	32	(as above)	(as above)	Sudo et al. (2002)
CAMchem	CESM1-CAM4-chemSD	1.9° x 2.5°	56	GEOS5 v5.2 meteorology	Deep convection is parameterized using the Zhang-McFarlane approach (Zhang and McFarlane, 1995), with some modifications, while shallow convection follows Hack et al. (2006)	Tilmes (2016)
GEOS5	v5	1.3° x 1.0°	72	MERRA	Convection is based on a modified version of the scheme described by Moorthi and Suarez (1992), which is a relaxed Arakawa-Schubert algoritm (RAS).	Rienecker et al. (2008) Colarco et al. (2010)
GEOSCHEMADJOINT	v35f	2.0° x 2.5°	47	GEOS-5 (MERRA)	Convective transport in GEOS Chem is computed from the convective mass fluxes in the meteorological archive, as described by Wu et al. (2007), which is taken from GEOS-5 (see above).	Henze et al. (2007)
EMEPrv48	rv4.8	0.5° x 0.5°	20	ECMWF's Integrated Forecast System (IFS) model	(see OsloCTM3 above)	Simpson et al. (2012)

Atmos. Chem. Phys. Discuss., doi:10.5194/acp-2016-443, 2016
Manuscript under review for journal Atmos. Chem. Phys.
Published: 10 June 2016

Atmospheric Chemistry and Physics Discussions
Open Access

Table 2: Regionally averaged burdens and climatological features for the six source regions. Burdens are multi-model median, annually averaged values for the *BASE* experiment with one multi-model standard deviation in parenthesis. Convective mass flux (for the layers between 1000 and 500 hPa), precipitation and cloud cover represent regionally and annually averaged values for 2010 from the Modern-Era Retrospective analysis for Research and Applications (MERRA) reanalysis data set.

	Region name	BC burden [mgm^{-2}]	OA burden [mgm^{-2}]	SO_4 burden [mgm^{-2}]	Convective mass flux [kgm^{-2}]	Precipitation [mm/day]	Cloud cover [%]
NAM	North America	0.36 (± 0.09)	3.86 (± 3.45)	3.55 (± 1.28)	3980	1.92	55
EUR	Europe	0.39 (± 0.09)	2.70 (± 1.83)	5.44 (± 1.43)	4774	1.89	53
SAS	South Asia	1.85 (± 0.36)	14.57 (± 7.67)	11.34 (± 3.57)	9769	3.34	43
EAS	East Asia	1.25 (± 0.26)	7.48 (± 4.17)	9.16 (± 2.43)	4105	1.89	46
RBU	Russia	0.29 (± 0.09)	2.84 (± 2.71)	4.58 (± 2.05)	2741	1.44	63
MDE	Middle East	0.41 (± 0.12)	3.43 (± 3.53)	11.54 (± 3.48)	1247	0.41	23

Atmos. Chem. Phys. Discuss., doi:10.5194/acp-2016-443, 2016
Manuscript under review for journal Atmos. Chem. Phys.
Published: 10 June 2016

Atmospheric Chemistry and Physics Discussions
Open Access

Table 3: Globally averaged radiative forcing from the six main experiments, weighed by the emission change for the given source region. Relative one standard deviations (representing multi-model variation) are given in parentheses.

	BC [$mWm^{-2}Tg^{-1}$]	**OA** [$mWm^{-2}Tg^{-1}$]	**SO_4** [$mWm^{-2}Tg^{-1}$]
NAMreduced	-51.9 (± 0.4)	7.9 (± 0.8)	4.5 (± 0.5)
EURreduced	-55.2 (± 0.4)	6.8 (± 0.6)	5.6 (± 0.4)
SASreduced	-93.8 (± 0.4)	10.2 (± 0.6)	7.9 (± 0.5)
EASreduced	-54.5 (± 0.3)	5.1 (± 0.5)	4.4 (± 0.3)
RBUreduced	-78.3 (± 0.6)	2.4 (± 2.2)	3.6 (± 0.3)
MDEreduced	-201.8 (± 1.6)	17.9 (± 0.4)	10.3 (± 0.7)

Atmos. Chem. Phys. Discuss., doi:10.5194/acp-2016-443, 2016
Manuscript under review for journal Atmos. Chem. Phys.
Published: 10 June 2016

Atmospheric Chemistry and Physics Discussions

Table 4: Response to Extra-Regional Emission Reductions (RERER), averaged over the 10 participating models. A high RERER value means that the given region is very sensitive to extra-regional emission reductions. The top table shows RERER for column aerosol burdens, the bottom table shows RERER for direct radiative forcing (DRF) calculated using vertically, spatially and temporally resolved AFE profiles.

Burden change	**NAM**	**EUR**	**SAS**	**EAS**	**RBU**	**MDE**
BC	0.51 ± 0.13	0.37 ± 0.06	0.12 ± 0.03	0.21 ± 0.05	0.83 ± 0.04	0.87 ± 0.04
OA	0.49 ± 0.19	0.41 ± 0.08	0.09 ± 0.03	0.24 ± 0.06	0.82 ± 0.06	0.90 ± 0.06
SO_4	0.46 ± 0.14	0.54 ± 0.09	0.36 ± 0.04	0.32 ± 0.07	0.75 ± 0.06	0.46 ± 0.08
DRF	**NAM**	**EUR**	**SAS**	**EAS**	**RBU**	**MDE**
BC	0.69 ± 0.11	0.57 ± 0.10	0.18 ± 0.04	0.37 ± 0.06	0.89 ± 0.03	0.91 ± 0.03
OA	0.46 ± 0.18	0.46 ± 0.08	0.09 ± 0.02	0.27 ± 0.06	0.83 ± 0.07	0.91 ± 0.06
SO_4	0.41 ± 0.12	0.53 ± 0.08	0.34 ± 0.04	0.31 ± 0.07	0.73 ± 0.05	0.47 ± 0.08